Journal of Coordination Chemistry
Publication details, including instructions for authors and subscription information:
http://www.tandfonline.com/loi/gcoo20

Synthesis, characterization, and antimicrobial activities of barbital-based alkaline earth metal complexes: the X-ray crystal structure of $[Ba_2H(Barb)_5]$ (Barb=5,5-diethyl barbiturate)

Mohamed M. Ibrahim [a b], Salih Al-Juaid [c], Mahmoud A. Mohamed [b d] & M.H. Yassin [e f]

[a] Chemistry Department, Faculty of Science, Kafr El-Sheikh University, Kafr El-Sheikh, Egypt

[b] Chemistry Department, Faculty of Science, Taif University, Taif, Saudi Arabia

[c] Chemistry Department, Faculty of Science, King Abdulaziz University, Jeddah, Saudi Arabia

[d] Biochemistry Department, Faculty of Agriculture, Cairo University, Cairo, Egypt

[e] Departement of Medical Microbiology, Faculty of Applied Medical Science, Taif University, Tarabah, Saudi Arabia

[f] Departement of Reproductive Diseases, ARRI, Giza, Egypt

Accepted author version posted online: 22 Jun 2012.Published online: 16 Jul 2012.

To cite this article: Mohamed M. Ibrahim, Salih Al-Juaid, Mahmoud A. Mohamed & M.H. Yassin (2012) Synthesis, characterization, and antimicrobial activities of barbital-based alkaline earth metal complexes: the X-ray crystal structure of $[Ba_2H(Barb)_5]$ (Barb=5,5-diethyl barbiturate), Journal of Coordination Chemistry, 65:17, 2957-2971, DOI: 10.1080/00958972.2012.705833

To link to this article: http://dx.doi.org/10.1080/00958972.2012.705833

Journal of Coordination Chemistry
Vol. 65, No. 17, 10 September 2012, 2957–2971

Synthesis, characterization, and antimicrobial activities of barbital-based alkaline earth metal complexes: the X-ray crystal structure of $[Ba_2H(Barb)_5]$ (Barb = 5,5-diethyl barbiturate)

MOHAMED M. IBRAHIM*†‡, SALIH AL-JUAID§, MAHMOUD A. MOHAMED‡¶ and M.H. YASSIN⊥‖

†Chemistry Department, Faculty of Science, Kafr El-Sheikh University, Kafr El-Sheikh, Egypt
‡Chemistry Department, Faculty of Science, Taif University, Taif, Saudi Arabia
§Chemistry Department, Faculty of Science, King Abdulaziz University, Jeddah, Saudi Arabia
¶Biochemistry Department, Faculty of Agriculture, Cairo University, Cairo, Egypt
⊥Departement of Medical Microbiology, Faculty of Applied Medical Science, Taif University, Tarabah, Saudi Arabia
‖Departement of Reproductive Diseases, ARRI, Giza, Egypt

(*Received 23 January 2012; in final form 7 May 2012*)

Three barbital-based alkaline earth metal complexes, $[Ca(Barb)_2]\cdot 3H_2O$ (**1**), $[Ba_2H(Barb)_5]$ (**2**) and $[Mg(Barb)_2]\cdot 2H_2O$ (**3**) (Barb = 5,5-diethyl barbiturate sodium salt), were synthesized and characterized with elemental analysis, thermal analysis, and infrared, Raman, ultraviolet, and NMR (^1H and ^{13}C) spectroscopies. Single-crystal X-ray diffraction studies reveal that **2** is a dimer. Each barium(II) is surrounded by an O_7N_2 donor set in an approximate monocapped square antiprism with Ba–O distances ranging from 2.6512(14) to 2.9168(15) Å and Ba–N distances of 2.7601(15) and 3.2558(17) Å. The complex forms polymeric networks in the solid state with different coordinating abilities of O and N donors and N–H···O hydrogen bonds. The antimicrobial activities of **1**–**3** were observed against different gram-positive and gram-negative bacteria, yeast, and molds. Variable antimicrobial activity against the different bacteria strains was observed and compared with that of standard antibiotics; minimum inhibitory concentration values ranged from 22 to 170 $\mu g\,mL^{-1}$ for bacteria.

Keywords: Antimicrobials; Barbital; Alkaline earth metal complexes; X-ray crystal structure; Therapeutics

1. Introduction

Compounds containing pyrimidine play an important role in many biological systems, where they exist in nucleic acids, vitamins, coenzymes, and antibiotics [1, 2]. Metal complexes of pyrimidine have been studied for their great variety of biological activities ranging from antimalarial, antibacterial, antitumoral, and antiviral [3–6]. Barbital, sodium 5,5-diethyl barbiturate, is one of the earliest barbiturates in medical use.

*Corresponding author. Email: ibrahim652001@yahoo.com

ISSN 0095-8972 print/ISSN 1029-0389 online
http://dx.doi.org/10.1080/00958972.2012.705833

Although it displays sedative-hypnotic activity [7], the biological consequence of its low lipid/water partition coefficient makes it interesting. A series of metal complexes involving barbitals has been prepared, in which the main interest is pharmacological activity that some barbiturates possess in *vivo*, blocking the excitation of membrane nerves. There is a controversy about whether the free acids [8] or the anionic forms [9] of barbiturates are more potent, and whether barbiturates interfere with the binding of calcium to phospholipids [10]. Thus, the interactions of barbiturates with calcium cations and water are of interest. The presence of several potential donors such as two amine nitrogen atoms and three carbonyl oxygen atoms makes barbitals interesting polyfunctional ligands (scheme 1). They have been used as building blocks in ordered organic supramolecular assemblies with directional hydrogen bonds [11–20], and they also are capable of bridging metal centers to form polymeric structures.

Alkaline earth elements are adsorbed on the surface of the cell wall of microorganisms and disturb the respiration of the cell, blocking the synthesis of the proteins that restrict further growth of the organisms. These metal(II) ions are essential for the growth-inhibitor effect. This inspired us to search for new barbital complexes with alkaline earth elements to assess the *in vitro* antimicrobial activity of alkaline earth elements associated with barbital against different strains of gram-positive bacteria (*Bacillus subtilis* and *Staphylococcus aureus*), gram-negative bacteria (*Escherichia coli* and *Salmonella typhimurium*), yeast (*Saccharomyces cerevisiae*), and molds (*Fusarium oxysporum*, *Rhizoctonia solani*, and *Macrophoma mangiferae*).

2. Experimental

2.1. *Materials*

Pure sodium 5,5-diethylbarbiturate (Barb) was obtained from Cipla Pharmaceutical Limited, India. Among the solvents employed, dimethyl formamide (DMF) and dimethyl sulfoxide (DMSO) were of spectroscopic grade. The nitrate salts of alkaline earth elements (Ca^{2+}, Ba^{2+}, and Mg^{2+}) were of Merck Chemicals.

2.2. *Instrumentation*

Infrared spectral measurements for ligand and metal complexes were recorded in KBr pellets using FT-IR Prestige-21 Shimadzu from 400 to 4000 cm^{-1}. Raman spectra were

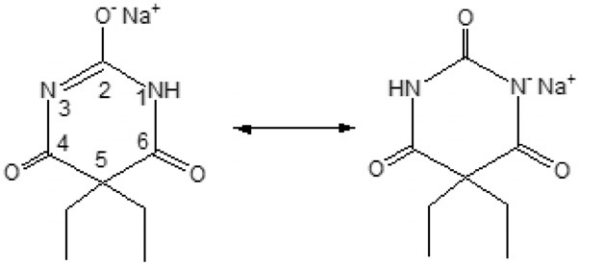

Scheme 1. The structure of the barbital ligand.

obtained as powders in glass capillaries on a Nicolet FT Raman 950 spectrophotometer. The spectra were recorded at room temperature with a germanium detector, maintained at liquid nitrogen temperature and using 1064.0 nm radiation, generated by a Nd-YAG laser with a resolution of 2 cm^{-1}. The conductivity measurements were carried out using Equiptronics digital conductivity meter model JENWAY 4070 type at room temperature for (1×10^{-3} mol L^{-1}) solutions. ^{1}H–^{13}C NMR spectra were taken for the ligand and complexes using a Varian 400-NMR spectrophotometer. The ^{1}H NMR spectra were recorded employing TMS as a reference and DMSO-d_6 as a solvent at ambient temperature. All UV-Vis measurements were recorded by a UV-1650pc Shimadzu. Thermal analyses of the complexes were recorded on a Netzsch STA 449F3 with system interface device in nitrogen. The temperature scale of the instrument was calibrated with high purity calcium oxalate. The operational range of the instrument was from ambient to 1200°C. Pure sample (5 mg) was used for dynamic TG scans at 10°C min^{-1}. SEM images with EDX were recorded on an Analytical Scanning Electron Microscope JEOL JSM-6390LA.

2.3. *General procedure for the synthesis of 1–3*

Complexes **2** and **3** were prepared by the method of Berking [21] for synthesizing calcium(II) complex **1**: aqueous solution of barbital (0.412 g, 2 mmol, 10 mL) was slowly added to each 10 mL of 1.0 mmol aqueous solution of respective metal(II) (Ca^{2+}, Ba^{2+}, and Mg^{2+}) nitrates with continuous stirring. The reaction mixture was refluxed for 2 h. The resulting solution was allowed to stand at room temperature and colorless crystals of **1**–**3** were obtained after 3 days.

2.4. *X-ray single-crystal determination of 2*

Crystallographic data (table 1) were collected on a Smart CCD diffractometer of Bruker AXS using Mo-Kα radiation. The crystal does not show significant intensity loss through data collection. Lorentz-Polarization corrections were performed by SAINT [22]. Absorption corrections were made by using SADABS [23]. The structures were solved by direct or Patterson methods using SHELXS-97 [24] to find the position of heavy atoms. Other non-hydrogen atoms were located by Fourier syntheses and refined using SHELXS-97 [24]. The least-squares refinements were performed using all independent reflections by the full matrix on F^2. All non-hydrogen atoms were refined anisotropically. Hydrogen atoms bonded to C and N were refined using a riding model, with C–H = 0.96–0.97 Å and N–H = 0.86–0.91 Å. The constraint Uiso(H) = 1.2 Ueq (C and N) or 1.5 Ueq (methyl C) was applied.

2.5. *Antimicrobial activity*

The antimicrobial activities of **1**–**3** were evaluated by the standard disc diffusion technique as described by Gillies and Dodds [25] and Ingolfsdottir *et al*. [26]. Species, strains and cultivation conditions of used microorganism are shown in table 2.

Table 1. Crystal data and structure refinement of **2**.

	Barium(II) complex **2**
Empirical formula	$C_{40}H_{56}Ba_2N_{10}O_{15}$
Formula weight	1191.63
Temperature (K)	100(2)
Wavelength (Å)	0.71073
Crystal system	Orthorhombic
Crystal color	Colorless
Crystal size (mm^3)	$0.52 \times 0.25 \times 0.08$
Space group	bpnm
Volume (Å^3), Z	4817.8(3), 4
Unit cell dimensions (Å, °)	
a	12.8539(5)
b	13.1771(5)
c	28.4440(11)
α	90
β	90
γ	90
Calculated density ($g\,cm^{-3}$)	1.643
Absorption coefficient (mm^{-1})	1.700
$F(000)$	2392
θ range for data collection (°)	1.74–25.09
Limiting indices	$-15 \le h \le 15$; $-15 \le k \le 14$; $-33 \le l \le 33$
Refinement method	Least-squares on F^2
Reflections collected	25,137
Independent reflection	4318 [R(int) = 0.0222]
Completness to θ (°)	98.7
Max. and min. transmission	0.8760 and 0.4718
Data/restraints/parameters	4318/0/331
Goodness-of-fit on F^2	1.093
Final R indices [$I > 2\sigma(I)$]	$R_1 = 0.0190$, $wR_2 = 0.0386$
R indices (all data)	$R_1 = 0.0220$, $wR_2 = 0.0398$
Largest difference peak and hole ($e\,Å^{-3}$)	0.339 and −0.448

Table 2. Strains and cultivation conditions of microorganisms.

Species of microorganisms	Strains	Cultivation conditions
Gram-positive bacteria		
G+ bacilli, spore-forming	*B. subtilis*[a]	TSA+YE, 30°C for 24 h
G+ cocci	*S. aureus* (ATCC 29213)	TSA+YE, 37°C for 24 h
Gram-negative bacteria		
G− short rods	*E. coli* (ATCC 25922)	TSA+YE, 37°C for 24 h
G− short rods	*S. typhimurium* (ATCC 19430)	TSA+YE, 37°C for 24 h
Yeast	*S. cerevisiae*[a]	TSA+YE, 30°C for 48 h
Mold	*F. oxysporum*[b]	PDA, 25°C for 72 h
	R. solani[b]	PDA, 25°C for 72 h
	M. mangiferae[b]	PDA, 25°C for 72 h

[a]Obtained from Department of Microbiology, Agriculture faculty, Cairo University.
[b]Obtained from Plant Pathology Institute, Agricultural Research Center, Egypt.
G+: Gram-positive bacteria, G−: Gram-negative bacteria, TSA+YE: Trypticase Soy Agar + 0.6% Yeast Extract, PDA: Potato Dextrose Agar.

2.5.1. Procedure. Target organisms were inoculated in melted (at 50°C) trypticase soy agar +0.6% yeast extract medium [27] and mold strains were inoculated in melted (at 50°C) potato dextrose agar medium [27] with heavy inoculum. Then the inoculated media were poured over a solid layer of uninoculated agar medium in

sterilized Petri-dishes and left to solidify at 4°C (surface layer should be constant in volume and horizontally homogenous). Discs of Whatman No. 1 filter paper (6.0 mm in diameter) were sterilized by autoclaving at 121°C for 15 min. An accurate weight of each compound (dissolved in DMSO 100 mg mL^{-1}) was aseptically added to each disc and left to dry. Each disc was aseptically placed on the middle of the agar surface (in triplicate) and left at 4°C for 1 h and then the plates were incubated. Gentamicin for bacterial strains and nystatin for fungal strains (10 μg per disc) were used as positive reference standards. The antimicrobial activities of target compounds were evaluated by measuring the average of inhibition zone diameters against the test microorganisms.

2.5.2. Determination of the minimum inhibitory concentration. Minimum inhibitory concentrations (MICs) of each target compound against the tested bacterial strains were determined by tube dilution using Trypticase soy broth +0.6% yeast extract [27, 28]. Inocula suspensions of the microorganisms were prepared from 12 h cultures. Each tested compound was dissolved in 10% DMSO and serial two-fold dilutions were prepared in sterilized tubes, ranging from 100 to 1000 μg mL^{-1}. The MIC was defined as the lowest concentration of compound which the microorganism did not demonstrate visible growth (visible turbidity).

2.5.3. Statistical analysis. Each of the measurements described was carried out in three replicate experiments and the results are recorded as mean ± standard deviation, calculated at level of $p \leq 0.05$.

3. Results and discussion

3.1. *Characterization of the alkaline earth metal complexes 1–3*

The reactions of nitrate salts of Ca^{2+}, Ba^{2+}, and Mg^{2+} with barbital in water in molar ratios of 2 : 1 at 50°C led to formation of three new complexes, $[Ca(Barb)_2] \cdot 3H_2O$ (**1**), $[Ba_2H(Barb)_5]$ (**2**) and $[Mg(Barb)_2] \cdot 2H_2O$ (**3**). The full reaction for the formation of **2** is represented in equation (1):

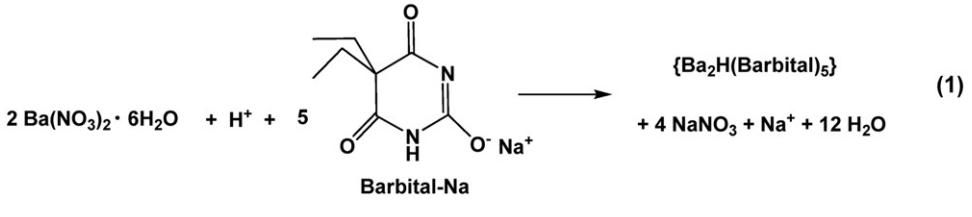

These complexes are stable solids and soluble in polar organic solvents, such as DMSO and DMF. Their melting points are above 230°C. Elemental analyses (table 3) are in agreement with the chemical formulas proposed for the compounds. Spectral techniques such as FT-IR, Raman, and ^{1}H–^{13}C NMR spectroscopies, as well as thermal studies (TG-DTG) and scanning electron micrographs (SEM-EDX), provide evidence for the proposed structures of the complexes. Scanning electron micrographs of **1**–**3**

Table 3. Molecular formulas, elemental analyses, and conductivities of the alkaline earth metal(II) complexes **1**–**3**.

Compound	Found (Calcd) %				$\Lambda_M(\Omega^{-1}\,cm^{-2}\,mol^{-1})$
	% C	% H	% N	% M	
$Ca(Barb)_2 \cdot 3H_2O$ (**1**) $C_{16}H_{28}N_4O_9Ca$	41.33 (41.73)	6.12 (6.13)	12.24 (12.17)	8.61 (8.70)	19.00
$Ba_2H(Barb)_5$ (**2**) $C_{40}H_{56}N_{10}O_{15}Ba_2$	40.95 (40.32)	4.69 (4.74)	11.90 (11.75)	23.41 (23.05)	34.00
$Mg(Barb)_2 \cdot 2H_2O$ (**3**) $C_{16}H_{26}N_4O_8Mg$	44.61 (45.04)	6.19 (6.14)	13.02 (13.13)	5.64 (5.70)	21.00

(Supplementary material) indicate the presence of well-defined crystals free from any shadow of metal ions on their external surface.

3.1.1. Infrared and Raman spectra. The IR and Raman spectral data of **1**–**3** are given in table 4. The IR (Supplementary material) and Raman (figure 1) spectra of **1**–**3** exhibit several sharp bands in the mid infrared region, clearly indicating the presence of barbital [29]. The strong and broad absorptions at 3541 and 3442 cm^{-1} in **1** and **3** are due to ν_{OH} of lattice water. The IR spectrum of **2** has no bands above 3187 cm^{-1}, indicating anhydrous nature of **2**. The spectrum below 3178 cm^{-1} is similar to that of **1** and **3**. The insignificant shifts of ν_{NH} in **1**–**3** as compared to ligand (3180 cm^{-1}) are at 3198, 3187, and 3151 cm^{-1}, respectively, probably due to formation of hydrogen bonds. The frequency range of 1736–1611 cm^{-1} is dominated by very strong IR and Raman bands arising from carbonyls. Change is observed for carbonyl vibrations $\nu_{C=O4,6}$ and ν_{C-O2}, diagnostic for its involvement in coordination. The $\nu_{C=O4,6}$ in **1** and **3** are observed as three distinct absorptions from 1657 to 1736 cm^{-1}, while **2** shows only two absorptions at 1684 and 1695 cm^{-1}. These observations are consistent with the presence of different carbonyls coordinated to metal, but the positions of the carbonyl bands in all complexes are comparable to each other. The $\nu_{C=O4,6}$ do not correlate predictably with coordination modes of this group. This may be due to the presence of strong intra- or intermolecular hydrogen bonding interactions [18], which affect the carbonyl bands, shifting them to lower frequencies. The ν_{C-O2} also shifted to lower frequencies (1484, 1489, and 1485 cm^{-1} for **1**, **2**, and **3**, respectively) compared to that of the ligand (1508 cm^{-1}). This indicates that the barbital anions are coordinated to metal *via* the carbonyl oxygen $O2^-$. This is further confirmed by the appearance of a medium intensity band at 407–592 cm^{-1} in spectra of the complexes, assigned to stretch of M–O [30] (table 4). A comparison of $\nu_{C=O}$ for **1**–**3** shows a decreasing trend from Mg^{2+} and Ca^{2+} to Ba^{2+}, attributed to increase the size of the metal cation, binding more weakly to the carbonyl oxygen of barbital. Raman spectrum of barbital exhibits two intense bands at 1611–1736 cm^{-1}, characteristic of $\nu_{C=O4,6}$. These bands show slight shift in all complexes. The presence of barbital anion in all complexes can also be confirmed by an intense band in the Raman spectrum at 653 cm^{-1}, assigned to ring breathing (ν_{ring}). This

Table 4. IR and Raman absorptions (cm^{-1}) and tentative assignment of the most important bands in barbital and **1**–**3**.

Barb-Na		$[Ca(Barb)_2]\cdot 3H_2O$ (**1**)		$[Ba_2H(Barb)_5]$ (**2**)		$[Mg(Barb)_2]\cdot 2H_2O$ (**3**)		Tentative assignments
IR	Raman	IR	Raman	IR	Raman	IR	Raman	
–	–	3541	–	–	–	3442	–	ν_{OH}
3180	3198	3152	3204	3187	3181	3151	3203	ν_{NH}
3058	2996	3060	2995	3059	2995	3089	2991	ν_{CH}
	2945		2956		2943		2942	
1695	1693	1698	1736	1696	1736	1696	1736	$\nu_{C=O,2,6}$
1664	1657	1670	1697	1684	1693	1671	1697	
	1611	1653	1657		1656	1650	1657	
1508	–	1484	–	1489	–	1485	–	ν_{C-O4}
1430	–	1416	–	1373	–	1383	–	δ_{CH}
1336	–	1339	–	1337	–	1338	–	δ_{NH}
1263	–	1281	–	1270	–	1238	–	ν_{CN}
840	653	872	644	840	653	866	655	ν_{ring}
–	–	554	548	592	533	552	507	ν_{M-O}
		494	495	502	486	491	455	
		454	455	470	455	458	407	

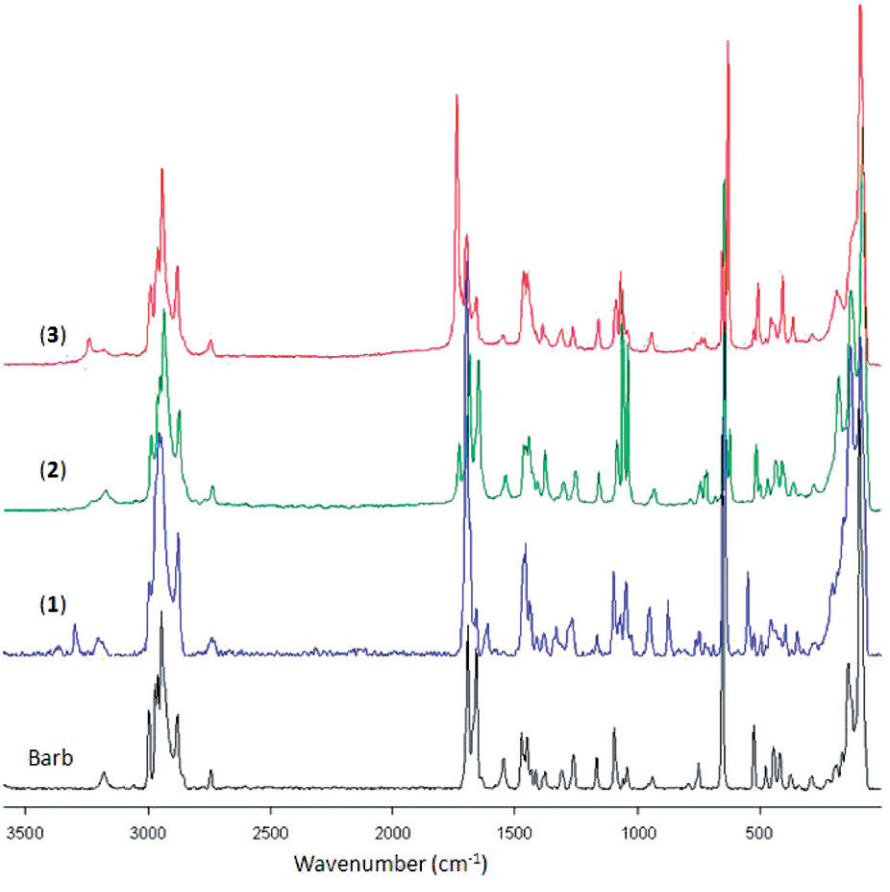

Figure 1. Raman spectra of **1**–**3**.

Table 5. ^{1}H–^{13}C NMR spectral data of **1–3** in DMSO-d_6.

	δ (–NH)	δ ($-H_2O$)	δ ($-CH_2$)		δ ($-CH_3$)		δ (–C–O$^-$)	δ (–C=O)
Complex	^{1}H	^{1}H	^{1}H	^{13}C	^{1}H	^{13}C	^{13}C	^{13}C
1	11.34 (s, 2H)	3.29 (s, 6H)	1.92 (q, 8H)	30.70	0.85 (t, 12H)	8.39	56.01	149.44 and 172.56
2	11.36 (s, 2H)	–	1.91 (q, 8H)	30.99	0.83 (t, 12H)	8.42	56.09	149.35 and 172.51
3	11.33 (s, 2H)	3.33 (s, 6H)	1.92 (q, 8H)	30.70	0.83 (t, 12H)	8.37	56.07	149.42 and 172.59

band is a specific marker for the presence of barbital [31]. Bands at 3060, 3059, and 3089 cm^{-1} for **1–3**, respectively, are due to ν_{CH}. Strong bands at 1416–1384 cm^{-1} in the complexes are due to δ_{CH} deformation, while ν_{CN} occurs as strong bands at 1281, 1270, and 1238 cm^{-1} for **1–3**, respectively. Raman spectra (figure 1) also give low frequency M(II)–O vibrations. The bands of most interest (248 and 175 cm^{-1}) are formed upon complexation, resulting from M(II)–O bonding. The M(II)–O band in **1–3** does not occur in the same position for all of the complexes, due to different mass of oxygen and the different bond strengths upon complexation.

3.1.2. Molar conductance. Molar conductance data in DMF at 10^{-3} mol L^{-1} are presented in table 3. The values lie in the range 19.0–34.0 Ohm^{-1} cm^{-2} mol^{-1}, which indicates that the barbital anions are coordinated to metal. The slightly higher values than those expected for non-electrolytes are probably due to partial replacement of the anion by strong donor solvent and the two species may exist in equilibrium. Therefore, the complexes may be considered as non-electrolytes.

3.1.3. NMR spectra. ^{1}H NMR spectral data of **1–3** (table 5) show expected signals of barbital. "Supplementary material" shows ^{1}H and ^{13}C NMR spectra of **1** as a representative example. Sharp signals at 11.34, 11.36, and 11.32 ppm are assigned to NH of barbital in **1–3**, respectively. These signals are downfield shifted compared to that of the ligand itself. Protons of water appear as a broad band at 3.29 and 3.31 ppm for **1** and **3**. The methyl and methylene protons in the ethyl show triplet and quartet peaks at 0.85 and 1.92 ppm for **1**; 0.84 and 1.95 ppm for **2**; and 0.85 and 1.91 ppm for **3**. ^{13}C NMR spectra for the barbital and **1–3** are in table 5. Almost every carbon in barbital is influenced, but C–O2$^-$ is significantly different from the other carbon atoms. These spectroscopic data reveal coordination of barbital *via* oxygen.

3.1.4. Electronic spectra. The spectral data obtained from UV-Vis spectroscopy are summarized in table 5. These spectra recorded in water yielded broad bands in the wavelength range of 270–275 nm. The λ_{max} was recorded as 277 nm for barbital,

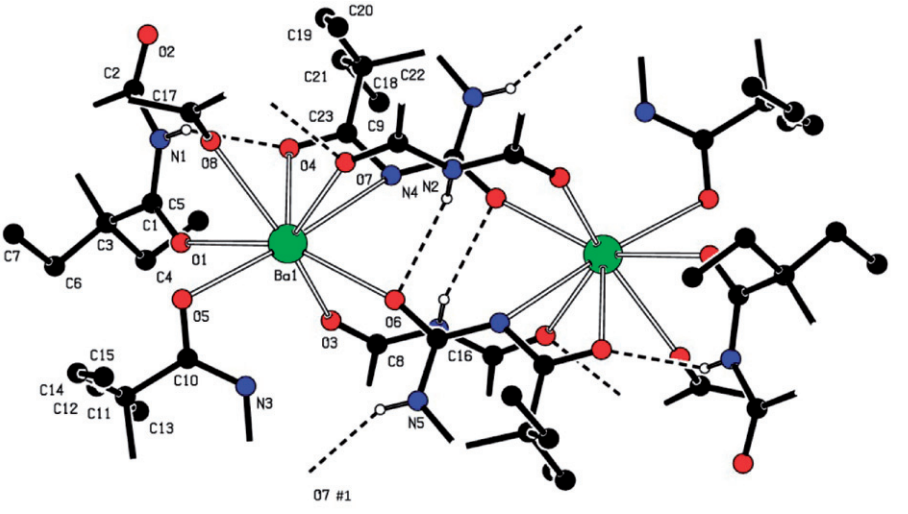

Figure 2. Solid presentation of single crystal X-ray structure of **2** showing the labeling scheme of non-hydrogen atoms. This structure is polymeric; six carbons (C2, C3, C4, C5, C6, and C7) and one oxygen (O2) are in the mirror plane and Ba1 and Ba1′ are generated by the centre of symmetry (−1). Inter and intramolecular hydrogen bonding is displayed.

attributed to a π–π^* transition. For complexes, red shifts were observed at 300–305 nm, due to bond formation to carbonyl.

3.1.5. Thermal analyses. Thermal analyses indicate that decomposition of **1**–**3** proceeds in several stages. The TG-DTG thermogram of **1** (Supplementary material) exhibits an endothermic event at 407.9 K accompanied by mass loss of 11.45% (Calcd 11.73%), assignable for removal of three water molecules of crystallization. The dehydration is followed by several decomposition processes with three strong exothermic events at 595, 688, and 755 K, accompanied by total mass loss of 51.63% (Calcd 51.71%), due to decomposition of 1.3 barbital, forming 0.4 mol of barbital and a mixture of $CaCO_3$ and CaC_2, which starts to decompose to form a mixture of CaO and CaC_2 as final solid product (Found 25.80%; Calcd 26.05%). Pyrolysis of **2** (Supplementary material) proceeds in three main stages. The first and second, 648–769 K, achieve a total mass loss of 51.93% (Calcd 52.77%). Thermal decomposition of **3** is identical to that of **1** with five distinguished steps. In all complexes, the experimental mass losses agree with the calculated values and the final decomposition product is a mixture of oxide and carbide. Based on DTG temperatures of decomposition of **1**–**3**, thermal stabilities depend on the central metal in the order Ba^{2+} (1157) > Mg^{2+} (1081 K) ~ Ca^{2+} (1081 K).

3.2. *Description of the crystal structure of 2*

The molecular structure of **2** with atom labeling is shown in figure 2. Selected bond lengths and angles are listed in table 6. In **2**, both bariums are nine-coordinate with

Table 6. Selected bond lengths (Å), angles (°), and hydrogen bond geometry of **2**.

Ba(1)–O(1)	2.9168(15)	O(3)–Ba(1)–O(6)	70.80(4)	O(4)–Ba(1)–O(1)	63.51(4)
Ba(1)–O(3)	2.6512(14)	O(3)–Ba(1)–O(5)	106.84(4)	O(8)–Ba(1)–O(1)	73.84(4)
Ba(1)–O(4)	2.7601(15)	O(6)–Ba(1)–O(5)	112.08(4)	O(7)–Ba(1)–O(1)	139.12(4)
Ba(1)–O(5)	2.6827(15)	O(3)–Ba(1)–O(4)	86.14(5)	O(3)–Ba(1)–N(4)	70.68(5)
Ba(1)–O(6)	2.6540(14)	O(6)–Ba(1)–O(4)	121.73(4)	O(6)–Ba(1)–N(4)	76.91(4)
Ba(1)–O(7)	2.7932(14)	O(5)–Ba(1)–O(4)	125.84(4)	O(5)–Ba(1)–N(4)	169.72(5)
Ba(1)–O(8)	2.7677(14)	O(3)–Ba(1)–O(8)	148.30(5)	O(4)–Ba(1)–N(4)	44.84(4)
Ba(1)–N(3)	3.2558(17)	O(6)–Ba(1)–O(8)	138.40(4)	O(8)–Ba(1)–N(4)	100.36(4)
Ba(1)–N(4)	3.0243(17)	O(5)–Ba(1)–O(8)	76.42(4)	O(7)–Ba(1)–N(4)	75.81(4)
		O(4)–Ba(1)–O(8)	68.15(5)	O(1)–Ba(1)–N(4)	101.60(5)
		O(3)–Ba(1)–O(7)	134.59(4)	O(3)–Ba(1)–N(3)	76.05(5)
		O(6)–Ba(1)–O(7)	72.46(4)	O(6)–Ba(1)–N(3)	74.01(4)
		O(5)–Ba(1)–O(7)	111.11(4)	O(5)–Ba(1)–N(3)	43.03(4)
		O(4)–Ba(1)–O(7)	91.21(4)	O(4)–Ba(1)–N(3)	150.90(5)
		O(8)–Ba(1)–O(7)	66.79(4)	O(8)–Ba(1)–N(3)	118.28(4)
		O(3)–Ba(1)–O(1)	78.27(4)	O(7)–Ba(1)–N(3)	117.70(4)
		O(6)–Ba(1)–O(1)	147.74(4)	O(1)–Ba(1)–N(3)	90.11(4)
		O(5)–Ba(1)–O(1)	68.15(5)	N(4)–Ba(1)–N(3)	141.37(4)
D–H···A	D(D–H)	*d*(H···A)	*d*(D···A)	∠(DHA)	
N(1)–H(1)···O(4)	0.73(3)	2.19(3)	2.728(2)	131(3)	
N(1)–H(1)···O(8)	0.73(3)	2.65(3)	3.218(3)	136(3)	
N(2)–H(2)···O(6)	0.82(2)	2.40(2)	3.099(2)	145(2)	
N(5)–H(5)···O(7)#1	0.82(3)	2.19(3)	2.920(2)	150(2)	

Symmetry transformations used to generate equivalent atoms: #1 $x+1/2$, $-y+3/2$, $-z+1$.

seven barbital oxygen atoms and two deprotonated barbital nitrogen atoms. The two Ba(II) ions are bridged by barbital dianions in an alternate up/down arrangement, leading to 1-D coordination polymers. The coordination can be pictured as distorted monocapped square antiprism around barium. All Ba–O bond distances are between 2.6512(14) and 2.9168(15) Å and the Ba–N distances are 2.7601(15) and 3.2558(17) Å. The barbital anions bridge the barium(II) cations through their carbonyl oxygen atoms. Barbital is monodentate and bidentate through carbonyl, while barbital with N5 is bidentate bridging *via* one carbonyl and a nitrogen. Eight-fold dodecahedron around barium has been found in the crystal structure of barium sulfonate chrysin coordination polymer [32, 33]. The greater formal negative charge seems to be equally distributed between two oxygen atoms adjacent to deprotonated nitrogen. Deprotonated nitrogen atoms are involved in hydrogen bonds or coordination with barium(II). The O(4) and N(4) distances for Ba(1) are 2.7601(15) and 3.2558(17) Å, respectively, forming O(4)–Ba(1)–N(4) angle of only 44.84° (instead of 72° for an ideal pentagon). Reduction of this angle from ideal may be due to intramolecular O(4)–N(4) distances, which are too short to allow more regular pentagons.

Each eight-coordinate Ba(II) in the polymeric chain is H-bonded to neighboring complexes (figure 3) in the polymeric chain with two varieties of H-bonding interactions. All hydrogen atoms attached to pyrimidine nitrogen function as H-donors and the free pyrimidine carbonyl O6 is a H-acceptor. Thus, each Ba(II) in **2** is linked to other units with N–H···O bonds and a C–H···O interaction (table 6), linking parallel chains in a 2-D H-bonded network (figure 4). Structural information of many Ba(II) coordination polymers of varying dimensionalities permits comparative study of Ba(II) coordination polymers [33–35]. These coordination polyhedra are not

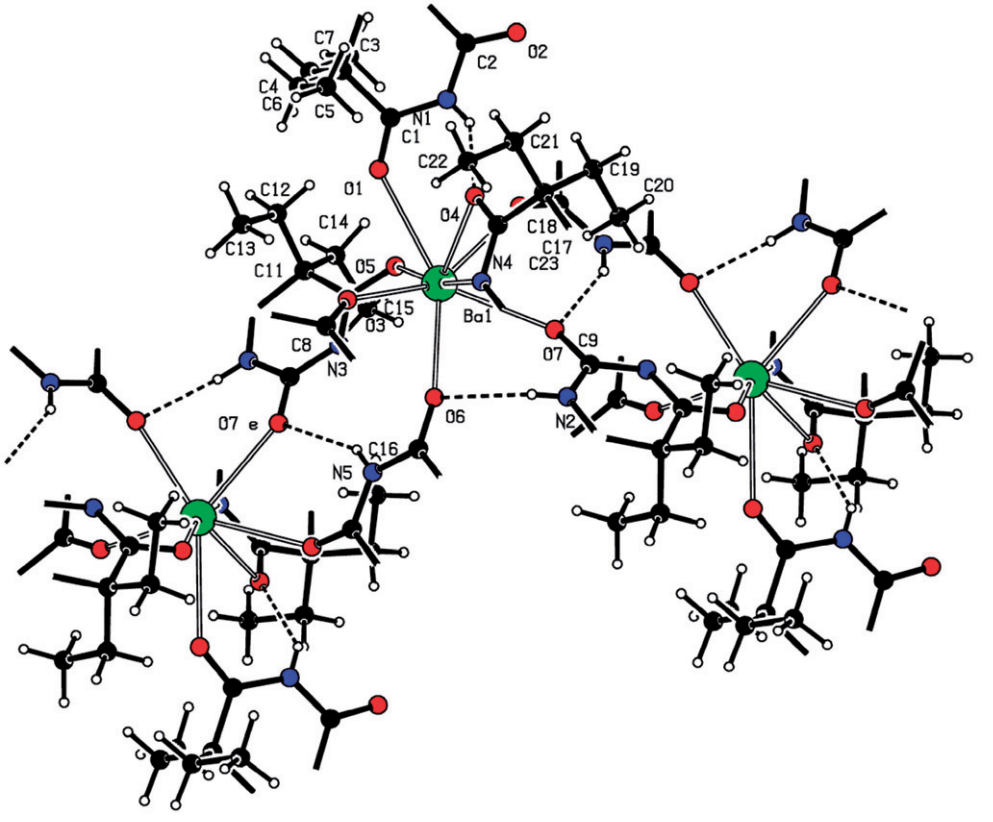

Figure 3. Projection along the *c*-axis, describing the geometry in the ribbons that are formed from **2**.

interconnected, but interact with the anions in ribbons and sheets establishing 3-D packing. The Ba···Ba distance across the polymeric chain varies from 4.069(2) in the 3-D coordination polymer derived from 2,2′-dithiobis(benzoic acid) to 7.467 Å in the 1-D Ba(II) polymer derived from the N-substituted amino acid containing the N-(6-amino-3,4-dihydro-3-methyl-5-nitroso-4-oxopyrimidin-2-yl) group. In all these compounds, carboxylates function as bridging ligands. The coordination number of Ba(II) varies from 8 to 10 with nine coordination observed in several compounds. In four of the polymers, the Ba···Ba separations are shorter than the sum of the van der Waals radii (4.28 Å) indicating weak metal–metal interactions, while in other compounds the observed metal–metal contacts are longer. The Ba···Ba distance of 4.5406(15) Å in **2** is much shorter than the Ba···Ba separation of 6.750(1) Å in the 1-D polymer $[Ba(H_2O)_5(4\text{-nba})_2]_n$ [36], derived from 4-nitrobenzoic acid where the nitro group is *trans* to carboxylate. The polymeric complex $[Ba(H_2O)_5(4\text{-nba})_2]_n$ contains two unique 4-nba ligands, one of which functions as a bidentate ligand with the other a bridging bidentate ligand. In the Ba(II) polymer of 4-nba, oxygen atoms of nitro group are not involved in coordination unlike **2**. Hence, it appears that the Ba···Ba distance in Ba–O coordination polymers is determined by a combination of several factors, which include the electronic and steric requirements of the central metal, the denticity, flexibility, bridging behavior, and H-bonding characteristics of carbonyl.

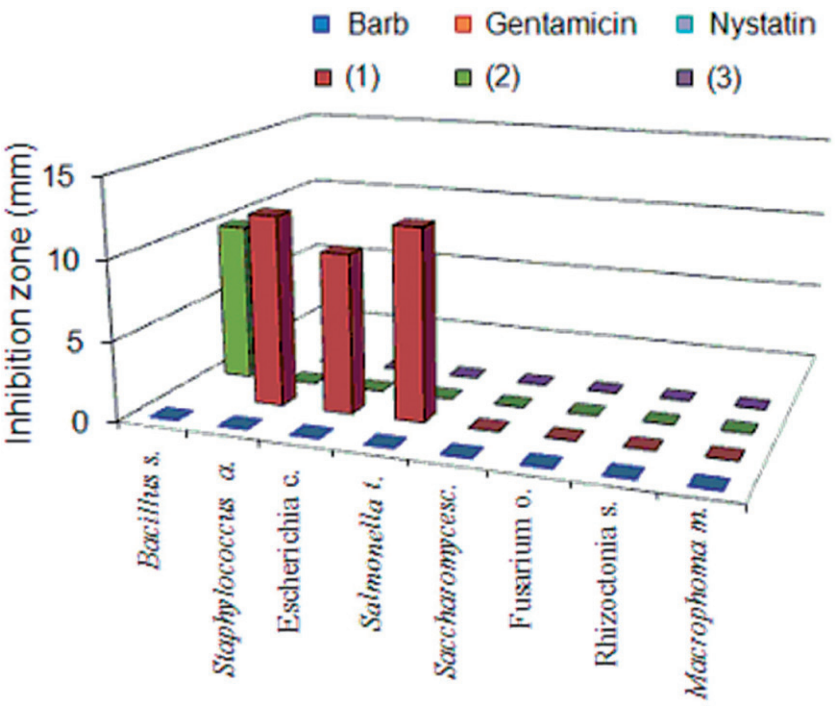

Figure 4. Inhibition zone (mm) of **1**–**3** and standard references against the target microorganism.

3.3. *Antibacterial activities*

The rate by which microorganisms develop resistance against antibiotics and chemotherapeutics is overtaking the development of new drugs for treatment of infectious diseases. Attention has focused on barbiturates, and other agents with affinities to cellular transport systems or agents showing other inhibition mechanisms [37–40]. Antimicrobial activity of each tested compound was observed by agar disc diffusion technique against gram-positive (*B. subtilis* and *S. aureus*) and gram-negative (*E. coli* and *S. typhimurium*), yeast (*S. cerevisiae*) and three strains of mold (*F. oxysporum*, *R. solani* and *M. mangiferae*). Results are presented in table 7 and figure 4. Complexes **1**–**3** display variable antibacterial activity against bacterial strains while barbital is not active against the microbes tested compared with standard antibiotics. Barbital-containing calcium(II) complex **1** showed a maximum % inhibition of 60%, 52%, and 48% compared with that of Gentamicin antibiotic against *S. aureus*, *E. coli*, and *S. typhimurium*. Complex **2** showed a maximum % inhibition of 30%, 57%, and 52% compared with that of Gentamicin antibiotic against *B. subtilis*, *E. coli*, and *S. typhimurium*. According to MIC values (table 8 and figure 5), **1** was more effective (has lowest concentration to be affective against microorganism) followed by **3**, while **2** was effective against *B. subtilis* only. These results indicate that binding of alkaline earth metal ions to barbital converted its clinical properties from anxiolytics and hypnotics to antibacterial substances.

Table 7. The zone of inhibition (mm) of barbiturate, **1**–**3**, Gentamicin, Nystatin, and DMSO.

	Zone of inhibition (mm)						
Species of organisms	Barb	**1**	**2**	**3**	Gentamicin	Nystatin	DMSO
Gram-positive bacteria							
B. subtilis	–		10	7	23	–	–
S. aureus	–	12	–	–	20	–	–
Gram-negative bacteria							
E. coli	–	10	–	11	19	–	–
S. typhimurium	–	12	–	13	25	–	–
Yeast							
S. cerevisiae	–		–	–		22	–
Mold							
F. oxysporum	–	–	–	–	–	16	–
R. solani	–	–	–	–	–	14	–
M. mangiferae	–	–	–	–	–	12	–

– denotes no inhibition.

Table 8. The MIC mean ± SD values ($\mu g\,mL^{-1}$) of the barbital and **1**–**3**, including Gentamicin.

	MIC ($\mu g\,mL^{-1}$)				
Species of organisms	Barb	**1**	**2**	**3**	Gentamicin
B. subtilis			119.2 ± 5.1	225.2 ± 5.1	15.2 ± 2.2
S. aureus		110.5 ± 2.9		150.1 ± 3.2	33.5 ± 3.5
E. coli		130.2 ± 4.7		170.2 ± 2.1	65.2 ± 3.1
S. typhimurium		145.2 ± 8.2			61.8 ± 8.5

The higher inhibition of microbial growth may also be due to uncoordinated hetero atoms. In the complexes, the barbital has some uncoordinated donors which enhance the activity of the complexes by bonding with trace elements present in microorganisms.

4. Conclusion

The presence of complexing ligand may affect the bioavailability of a metal in blood or tissues. Therefore, to study the interaction of barbital with alkaline earth elements present in human body, barbital has been reacted with nitrate salts of Ca^{2+}, Ba^{2+}, and Mg^{2+} in Barbital : M ratio of 2 : 1 forming three complexes, $[Ca(Barb)_2]\cdot 3H_2O$ (**1**), $[Ba_2H(Barb)_5]$ (**2**), and $[Mg(Barb)_2]\cdot 2H_2O$ (**3**). These complexes were spectroscopically characterized by using FT-IR, Raman, and ^1H NMR spectroscopies. The crystal structure of the dimeric barium barbital **2** showed that each barium is surrounded by an O_7N_2 donor set in approximate monocapped square antiprism environment.

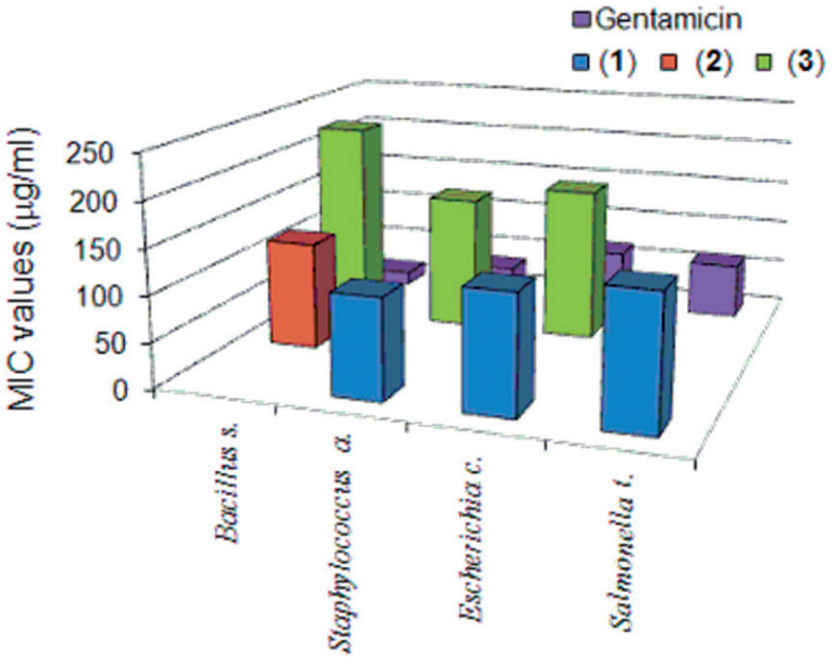

Figure 5. MIC values of **1**–**3** and standard references against the target microorganism.

A comparative study of inhibition of barbital and its alkaline earth metal complexes **1**–**3** against gram-positive (*B. subtilis* and *S. aureus*) and gram-negative (*E. coli* and *S. typhimurium*), yeast (*S. cerevisiae*), and three strains of mold (*F. oxysporum*, *R. solani*, and *M. mangiferae*) indicates that the complexes exhibit higher antimicrobial activities than the free drug. These results indicate that binding of alkaline earth metals to barbital are essential for growth-inhibitor effect, which convert its clinical properties from anxiolytics and hypnotics to antibacterial substances. Therefore, this study is developing a modular form of barbital based on its interaction with alkaline earth ions as effective antibacterial substances.

Acknowledgments

The authors acknowledge financial support by Taif University, Saudi Arabia.

References

[1] F. Hueso-Urena, N.A. IIIan-Cabeza, M.N. Moreno-Carretero, J.M. Martinez-Martos, M.J. Ramirez-Exposito. *J. Inorg. Biochem.*, **94**, 326 (2003).
[2] M.S. Refat, S.A. El-Korashy, A.S. Ahmed. *Spetrochim. Acta*, **71A**, 1084 (2008).
[3] E.S. Raper. *Coord. Chem. Rev.*, **61**, 115 (1985).

[4] J.S. Casas, E.E. Castellans, M.D. Louce, J. Ellena, A. Sanchez, J. Sordo, C. Taboada. *J. Inorg. Biochem.*, **11**, 1858 (2006).
[5] M.J. Campbell. *Coord. Chem. Rev.*, **15**, 279 (1975).
[6] M.C. Rodriguez-Argüelles, M.B. Ferrari, G.G. Fava, C. Pelizzi, P. Tarasconi, R. Albertini, P.P. Dall'Aglio, P. Lunghi, S. Pinelli. *J. Inorg. Biochem.*, **58**, 157 (1995).
[7] J.H. Block, J.M. Beale. *Wilson and Gisvold's Textbook of Organic Medicinal and Pharmaceutical Chemistry*, 11th Edn, Lippincott Williams & Wilkins, Philadelphia (2004).
[8] H.P. Blaustein. *J. Gen. Physiol.*, **51**, 293 (1968).
[9] S.K. Sharpless. In *Pharmacological Basis of Therapeutics*, L.S. Goodman, A. Gillman (Eds), 3rd Edn, pp. 109–116, Macmillan, New York (1968).
[10] P. Kripp, C.P. Bianchi, G. Suarez-Kurtz. *J. Pharm. Pharmacol.*, **21**, 763 (1969).
[11] J.-M. Lehn, M. Mascal, A. Decian, J. Fischer. *J. Chem. Soc., Chem. Commun.*, 479 (1990).
[12] K.C. Russell, J.-M. Lehn, N. Kyritsakas, A. DeCian, J. Fischer. *New J. Chem.*, **22**, 123 (1998).
[13] P.V. Bernhardt. *Inorg. Chem.*, **38**, 3481 (1999).
[14] F. Yilmaz, V.T. Yilmaz, E. Bicer, O. Buyukgungor. *Z. Naturforsch.*, **61b**, 275 (2006).
[15] V.T. Yilmaz, F. Yilmaz, H. Karakaya, O. Buyukgungor, W.T.A. Harrison. *Polyhedron*, **25**, 2829 (2006).
[16] F. Yilmaz, V.T. Yilmaz, E. Bicer, O. Buyukgungor. *J. Coord. Chem.*, **60**, 777 (2007).
[17] F. Yilmaz, V.T. Yilmaz, H. Karakaya, O. Buyukgungor. *Z. Naturforsch.*, **63b**, 134 (2008).
[18] V.T. Yilmaz, M.S. Aksoy, O. Sahin. *Inorg. Chim. Acta*, **362**, 3703 (2009).
[19] M.S. Aksoy, V.T. Yilmaz, O. Buyukgungor. *J. Coord. Chem.*, **62**, 3250 (2009).
[20] V.T. Yilmaz, E. Soyer, O. Buyukgungor. *J. Organomet. Chem.*, **694**, 3306 (2009).
[21] B. Berking. *Acta Cryst.*, **B28**, 98 (1972).
[22] SAINT, *V6.02*, Bruker AXS, Madison, WI (1999).
[23] G.M. Sheldrick. *SADABS, Area-Detector Absorption Correction*, Göttingen, Germany (1996).
[24] G.M. Sheldrick. *Program SHELXS, Program for Crystal Structure Determination*, Göttingen, Germany (1997).
[25] R.R. Gillies, Dodds. *Bacteriology Illustrated*, 5th Edn, Churchill Livingstone, Edinburgh, London, Melbourne and New York (1984).
[26] K. Ingolfsdottir, M.A. Hjalmarsdottir, A. Sigurdsson, G.A. Gudjonsdottir, A. Brynjolfsdottir, O. Steingrimsson. *Antimicrob. Agents Chemother.*, **41**, 215 (1997).
[27] APHA. *Standard Methods for the Examination of Dairy Products*, 17th Edn, American Public Health Association Inc., Washington, DC (1987).
[28] W.C. Evans. *Trease and Evan's Pharmacognosy*, 14th Edn, W.B. Saunders, London (1996).
[29] M.S. Refat, T. Sharshar. *J. Mol. Struct.*, **1016**, 140 (2012).
[30] A.R. Timerbaev, C.G. Hartinger, B.K. Keppler. *TrAC Trends Anal. Chem.*, **25**, 868 (2006).
[31] H.C. Garcia, F.B. De Almeida, R. Diniz, M.I. Yoshida, L.F.C. De Oliveira. *J. Coord. Chem.*, **64**, 1125 (2011).
[32] Z. Zhang, J. Shi, Y. He, Y. Guo. *Inorg. Chem. Commun.*, **9**, 579 (2006).
[33] A.L. Spek. *J. Appl. Cryst.*, **36**, 7 (2003).
[34] R. Murugavel, K. Baheti, G. Anantharaman. *Inorg. Chem.*, **40**, 6870 (2001).
[35] B.H. Lee, C.H. Kim, S.G. Lee. *Acta Crystallogr.*, **C59**, 196 (2003).
[36] B.R. Srinivasan, S.Y. Shetgaonkar, P. Raghavaiah. *J. Chem. Sci.*, **120**, 249 (2008).
[37] J.E. Kristiansen, L. Amaral. *J. Antimicrob. Chemother.*, **40**, 319 (1997).
[38] H. Cederlund, P.A. Mårdh. *J. Antimicrob. Chemother.*, **32**, 355 (1993).
[39] A.N. Chakrabarty, J. Molnar, S.G. Dastidar, N. Motohashi. *Non Antibiotics: A New Class of Unrecognized Antimicrobics*, National Institute of Science Communication, New Delhi, India (1998).
[40] S. Tyski. *Acta Pol. Pharm.*, **60**, 401 (2003).